Transiting Exoplanet in the Near Infra-red for the XO-3 System

Nathaniel Rodriguez

August 26, 2009

Abstract

Our research this summer focused on determining if sufficient precision could be gained from WFCAM test data to detect the secondary eclipse of a transiting exoplanet in the near-infrared. We approached our required precision for detecting the secondary eclipse using aperture photometry and a differential photometry algorithm. We managed to detect the egress of the primary eclipse for our target star, XO-3, and found that the systematic error limit could be reached with only around 150-200 stars in an image, possibly even less. This result shows that the full field-of-view offered by the UKIRT telescope is unnecessary for reaching maximum precision. This suggests that other non-survey telescopes could be used that may be better suited to the project and would offer more available narrowband filters in the near-infrared.

1 Introduction

The purpose of this research was to determine various properties of transiting exoplanets in the near-infrared using ground based telescopes. To date there have been 365 confirmed exoplanet detections. Of these only a small portion have observable eclipses, due to the relatively low probability of the exoplanet's orbit being oriented correctly. Observing transits provides the best opportunity to learn more about these systems than would otherwise be possible. Characteristics such as planet radius, atmospheric temperature and composition, and orbital inclination can be determined through direct observation of transits (2). The research focuses on secondary transit observations in the near-infrared. The secondary transit in particular provides insight into most of the properties of the planet, many of which can not be determined through the primary transit. However, detecting the secondary transit requires greater precision than the primary, as the depth of the secondary is much shallower. This summers projects goal was to show that the research is worthy of dedicated telescope time. To do this we developed methods of reducing the error to a tenth of a percent or less, which is sufficient to detect the secondary eclipse.

2 Background

2.1 Transits

There are a number of various methods that can be used for detecting extra-solar planets such as astrometry, radial velocity, pulsar timing, transits, gravitational microlensing, circumstellar disks, and direct imaging. Some of these techniques are considerably more effective than others and have resulted in actual detections of extra-solar planets. The radial velocity method is by far the most effective at finding new planets. It takes advantage of the star's wobble about the center of mass caused by a closely orbiting object. By measuring the Doppler shift in the stars spectrum one can detect the presence of an object (1). This method is effective for finding systems where the orbiting object is fairly massive and its orbital period is very short. The XO-3 system is an example of such a case. The exoplanet in this system has a mass of 11.8 M_J and an orbital period of just over 3 days. The vast majority of the 365 known exoplanets were found through this technique. However, the radial velocity method, while effective at finding new systems that contain exoplanets, can only provide us with an estimate of the mass of the orbiting object (since its orbital inclination is unknown). To learn more about the planet other techniques must be used.

The transit method of detection can tell us a great deal about the planets that have already been discovered. A transit occurs if the exoplanet's orbital inclination causes it to pass between the parent star and the observer. Depending on the size of the planet and its distance to the star a certain portion of the stars light will be blocked off. If the star is being observed during this time a noticeable decrease in flux is detected from the system. This is known as the primary eclipse. The secondary eclipse occurs when the planet passes behind the star. Both the star and the planet behave as blackbodies, so they emit radiation according to their temperature. The star is detected as a point

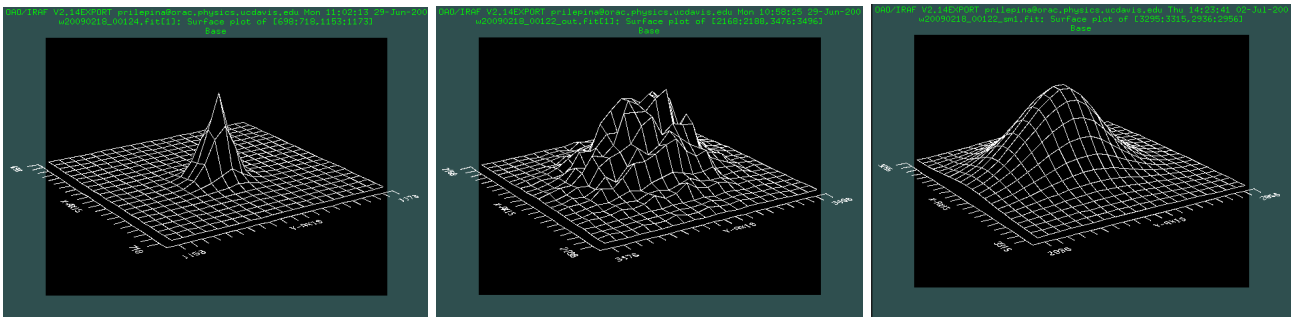

(a) (b) (c)

Figure 1: Graphs comparing the surface plots for a star in an raw image (a), composite image (b), and smoothed image (c). (a) Shows the surface plot of a star in a raw exposure. They are essentially point sources with a Gaussian distribution and a small FWHM. (b) The distribution of the same star in one of the composite images. It is visibly apparent that the star does not exhibit the properties of a point source. There are local maximums and minimum scattered throughout the distribution. This unusual architecture likely resulted from the combination of the dithered images. It caused the algorithms we used in IRAF that find stars on an image to detect additional sources within a star, resulting in multiple detections of the same star in slightly different places. (c) A 2-D Gaussian smoothing algorithm was applied to all the composite images so that star finding tools could be applied to them without creating multiple or false detections. This surface plot shows how the result of the smoothing on the same star.

source on the detector, so the light received by the detector comes from the whole system. When the planet passes behind the star its light is no longer visible which results in a small drop in the flux of the system. During an orbital period there will be both a primary eclipse, and a much smaller secondary eclipse. Using the secondary eclipse you can subtract the flux of the system from that of the star (as the planet is no longer contributing) leaving the flux contribution due to the planet alone. It is this idea that opens the path for determining additional characteristics of the planet.

3 Instrumentation

The test data came from the Wide Field Infrared Camera (WFCAM) on UKIRT. The device was designed to carry out large-scale survey observations, but time is provided for other projects as well. It has four separate detectors that cover a total area of 0.75 sq degrees (4). A narrowband 2.12 micron filter was used (H2 1-0 S1) for our exposures. Longer wavelength filters are preferable because the contrast between the parent star's light and the planet's increases with wavelength, resulting in a deeper and more pronounced well in the light curve[1]. However, the wavelength can not be made too long due to emissions from the Earth and its atmosphere. After about 3 microns the atmosphere and Earth emit considerable amounts of radiation that reduce the data's signal to noise ratio, sufficient to make secondary transit detection more difficult and less precise. Emissions from the instrument itself are insignificant and easy to correct for since it is cooled to a temperature of about 70K.

The test data employed a dithering technique where each image is a composite of nine separate exposures that are shifted by a small amounts (± 8 arcsec). Combining exposures was used to increase the signal-to-noise ratio without increasing the exposure time (which could result in saturating the image). By combining two exposures you can effectively double the signal, while the noise which is random, only increases by a factor of $\sqrt{2}$. The dithering takes care of pixel defects, such as hot and cold pixels.

Stars in the composite images showed unusual internal architecture that was not expected of point sources. These effects were likely artifacts caused by combining the dithered exposures. To eliminate this effect the images were smoothed using a 2-D Gaussian.

What we found was that the stars in these stacked images had distributions that were not synonymous with point sources (see Figure 1.a). The dithering caused multiple peaks and local maximums within most stars. As

[1] A light curve is a plot of the differential magnitude (or relative flux) of a star with respect to time. These plots show how the magnitude of the star changes over the course of an observation. In term of planetary transits the light curve is generally plotted with the magnitude axis displaying ratios of the maximum brightness (being 1.0) and the time axis displaying time with respect to the phase of the transit (with 0 being the mid-transit).

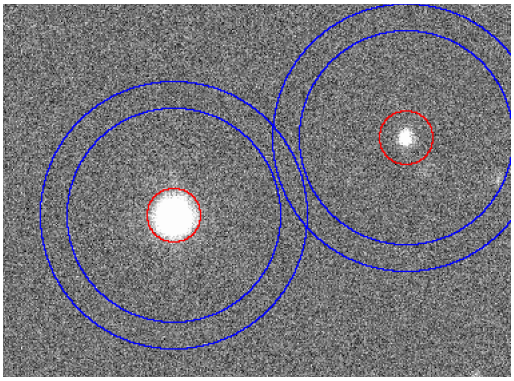

Figure 2: A section of one of the composite images from our data set. The red circle represents the aperture and the blue circles represent the inner and out annuli. The aperture fits the larger star very well but is slightly oversized for the smaller star. We used a single aperture size throughout the image because the differential photometry algorithm weighs against stars of higher variability and S/N, which are generally the smaller, dimmer stars.

a result the star finding algorithm that was used to make star-lists (daofind), detected multiple sources within what was obviously a single source. To deal with this abnormality the images were smoothed using a 2-d Gaussian smoothing algorithm (see Figure 1.c).

The images we received were targeted at the XO-3 system, where there is a well documented transiting exoplanet. Forty-five images (fifty minutes worth) were taken during the egress (the end of the transit) of the primary eclipse. Since UKIRT receives a very large amount of data in a night it is reduced on site before it becomes available. So each of the exposures we received were reduced data that already had corrections done for flat fielding, dark noise, and debiasing.

4 Methods

To accomplish the task of reaching milli-magnitude precision we used IRAF to accomplish all of the aperture photometry. For the differential photometry we used an algorithm developed by Christopher Broeg, et al (2004).

4.1 Aperture photometry

The purpose of aperture photometry is to determine the instrumental magnitude of the stars in an image. In a CCD exposure each pixel has an integer number of counts (related to the number of electrons ejected by incident photons). By drawing a closed surface (usually a circle) around a star and summing over the number of counts you can determine the flux through that surface (where I is the count for each pixel):

$$F_T = \sum_i I_i$$

When choosing an aperture size for a star it is common to pick values that are 2-5 times the FWHM (full-width half-maximum) of the stars point source distribution (5). If the aperture is too large it may include other stars or degrade the signal-to-noise ratio of dimmer stars. Therefore, it is generally good practice to make sure that the aperture fits snugly around the star (see Figure 2).

In our case we chose to use a single aperture size for all of the stars in each image and from each detector. There are two reasons for this choice. The first is that by using the same aperture size for all the stars in all four detectors, we can determine and correct for systematic differences between the detectors. Without this it would not be possible to use stars from other detectors in the differential photometry, and by correcting for these differences a master star list can be compiled and compared to actual magnitudes from a sky-survey. The second reason is that using variable apertures is much more tricky to do. It adds additional complications that for an analysis of test data would be unnecessary. The downside of course to this method is that it forced us to use an aperture size that would fit the target star (XO-3) which was a comparatively large and bright star. This meant that while the brighter stars in each image were not affected, most of the dimmer stars would have apertures of 10-30 times larger than their FWHM adding a considerable amount of noise to an already noisy object. While this may seem potentially dangerous in our attempt to maximize precision, due to the algorithm we use for the differential photometry, it in

fact does not affect us at all.

After the aperture size is chosen for a star, the next step is to chose a size for the sky annuli, which are used to take a sample of the local sky background. Generally the inner sky annulus is chosen to be around 4-5 times the aperture radius and the outer sky annulus about 6-7 times the aperture radius (5). The mean background value is then calculated from the sky annuli. IRAF uses a robust algorithm to do this, so that the presence of stars or other background features within the sky annuli do not effect the result. This mean value is then used to subtract out the flux due to the background in the aperture, leaving only the flux due to the star (where B is the mean sky background value, and N is the number of pixels within the aperture):

$$F = \sum_i I_i - N\tilde{B}$$

The insturmental magnitude can then be calculated from the flux:

$$M_I = -2.511886 \log \left(\sum_i I_i - N\tilde{B} \right)$$

4.2 Differential photometry

Ground based observations have the added complication of atmospheric disturbances to deal with. Variations in the amount of air between the observer and space (the air mass) effects the brightness of the object being observed, an effect known as extinction. If observations are done directly overhead the air mass is at its minimum resulting in less scattering and absorption of light. If observations are done near the horizon air mass is at its maximum as the light from the object must pass through more particles in the atmosphere before reaching the observer. Extinction causes systematic errors for time-series exposures that track an object across the sky for prolonged periods of time. To correct for this error differential photometry is used.

The method for differential photometry is to chose a comparison star (CS) and subtract its magnitude from other stars in the image. The comparison star will have a zero magnitude for all exposures, and every other star will have a differential magnitude that is relative to the comparison star's magnitude. If we assume the comparison star's absolute magnitude does not change over the course of observation, and that each star in an exposure is being affected in a similar way by extinction, then any systematic error caused by changes in the atmosphere from one exposure to another will be canceled out due to the subtraction.

Ideally a CS should have a magnitude similar to target star's (the star you are tracking), and it's absolute magnitude should vary as little as possible (a variable star or a binary system should not be chosen as a CS). The magnitudes should be similar because the error of the target star will be estimated from the comparison star's rms deviation from its mean. A CS that is brighter or dimmer than the target will have a different signal-to-noise ratio and so different errors associated with it.

Since so much rests on choosing an appropriate comparison star, including precision, we used an algorithm developed by Christopher Broeg and others (2004), which takes a quantitative approach to choosing the optimal comparison star. The algorithm works by letting all stars in an image be used as comparison stars. It then uses a weight system that reduces the impact of highly variable and low signal-to-noise stars. The weight system effectively allowed us to use a single aperture size, since the aperture we chose favored brighter stars. The error of the target is then interpolated from a model that is fit to the observed variability of the data. This algorithm offers a number of advantages over the traditional method of doing differential photometry. Since the algorithm uses all stars as CS and weighs them accordingly there is no need to research the stars in the field-of-view, which would be required if comparison stars were to be chosen manually. It then creates an artificial CS which it uses as the reference for the differential magnitudes of the other stars.

4.3 Floor Reduction

The goal of the project was to show that errors could be reduced to a level which allows for secondary eclipse detection. The floor of the systematic error can be determined by graphing the standard deviation of the differential magnitude as a function of the star's differential magnitude (see figure 3). The floor essentially shows us the limit of our precision. This is what the differential photometry algorithm aims at reducing. By choosing optimal parameters for the algorithm, the floor can be reduced to its minimum level.

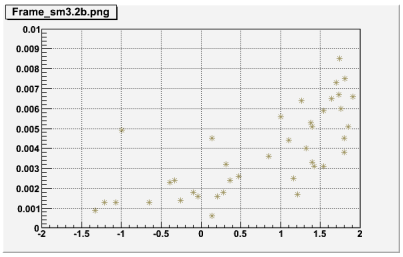

Figure 3: Dimmer stars have a lower signal-to-noise ratio, so their standard deviations vary considerably and tend to be high. The brighter stars on the other hand, have higher signal-to-noise ratios, so their standard deviation is smaller and approaches a certain minimum value. The error floor of the data is defined by this value. Towards the brighter (lower magnitude) end of the graph the standard deviations level off approaching this value which is around 0.001 mag. The target star, XO-3, is the star in the left portion of the plot with a magnitude of -1 and a standard deviation of 0.005 mag.

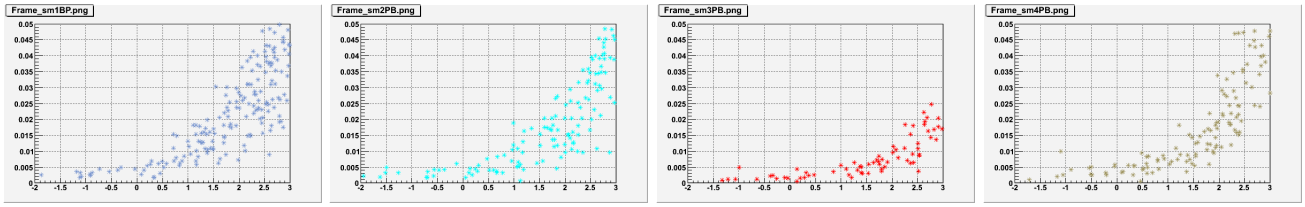

(a) Detector 1

(b) Detector 2

(c) Detector 3 (the target star, XO-3 is the -1 mag star with a higher deviation that the comparably bright stars)

(d) Detector 4

Figure 4: Graphs of the standard-deviation of the differential magnitude with respect to the differential magnitude.

5 Results

5.1 Floor

To determine the floor we made the appropriate plots of the standard deviation of the differential magnitude as a function of the differential magnitude. This was done for each detector individually, where the algorithm was ran using only the stars in that specific detector. Since the images were taken in one-minute exposures, and transits generally occur over several hours, one minute time resolution was unnecessary so the data was binned into nine-minute bins, decreasing the standard deviation of most stars by a factor of three.

The following four (see Figures 4.a - 4.d) plots show that the floor for each detector was at or below 0.0025 mag, with detector three having a floor at about 0.001 mag.

In principle using the Broeg algorithm provides better precision, hence lowering the floor to its minimum, if more stars are used as comparison stars. To test this, a master star list was created that included three of the detectors[2]. To use the stars from other detectors, inconsistencies between the detectors had to be corrected for. For instance, the instrumental magnitude determined for a star on one detector would most-likely be different if determined on one of the others. To correct for this error another sky survey was used which contained a catalogue of the absolute magnitudes of the stars in the near-infrared. The absolute magnitude of a number of stars was used to determine how each detector should be corrected. The resulting differential photometry for this list of stars is shown in Figure 5.

This plot shows that there is no significant drop in the floor from that of the individual detectors. So there is no difference between using 762 stars (the number used in the master-list) or only 282 stars (number used in detector 1). We then attempted to find how many stars were needed to determine with confidence what the minimum attainable error was. To do this a variable number of stars were randomly removed from a detector and the differential photometry was calculated using the remaining stars. While it is not yet fully conclusive, only 150-200 may be needed to confidently reach the floor, possibly less. The number depends on how many bright stars are present,

[2]Detector three was left out due to an issue with the dphot program calculating the differential magnitudes of its stars.

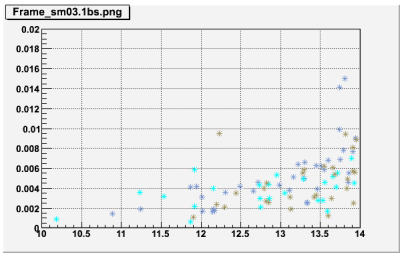

Figure 5: The combined star list does not have an appreciably lower floor than the individual detectors. This means that the systematic error has been reduced to its minimum, which suggests that having a field of view as large as the UKIRT telescope offers is not necessary since having additional stars does not provide any benefit. By removing stars from the individual detectors we have determined that the floor can be reached with confidence by 150-200 stars, though this value could be dropped down even lower depending on the number and distribution of bright stars present in the field-of-view.

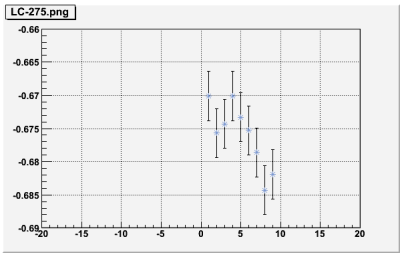

Figure 6: The light curve is plotted as a function of the differential magnitude with respect to binned time. So each tick represents five-minutes. The magnitude of the target star drops over the course of the observation so the star is getting brighter, which is suggestive of the egress of the transit. This was confirmed by checking the observation times with previous eclipses.

and how they are distributed.

5.2 Transit

The test data we acquired from UKIRT only covers a fifty-minute window so it was not possible to detect a full transit. However, the images were taken during the egress of the primary transit, which we were able to detect.

Figure 6 shows the light curve of the differential magnitude as a function of the exposure. The points show a trend in decreasing magnitude (increasing brightness) which is characteristic of what should be seen for the egress of a transit.

6 Discussion and Future work

To confirm that we had good data on the egress of the primary transit we will see how the data fits to a theoretical model of planetary transits given the particular parameters of XO-3b. This will tell us if our data meets with the expected values for the depth of the well in the near infrared and the duration of the egress.

Earlier it was pointed out that only 150-200 stars were needed to minimize the error. This result implies that using the WFCAM instrument would not be necessary to attain the required precision. If this is the case then a number of other telescope opportunities open up which could be used instead of UKIRT. Some possible options include using the ESO observatories in La Silla, Paranal, La Palma, or Spain which all have telescopes with narrowband filters in the near-infrared. Ideally the telescopes that we propose to will have multiple narrowband filters in the near-infrared around 2-3 microns. There are theoretical exoplanet atmospheric models that model the flux contrast between the star and planet as a function of the wavelength. Having multiple points from narrowband filters to fit it this model will tell us a great deal, either by agreeing with the model, or if not, what this means for the model.

While the XO-3 system was our original target we are looking for additional targets to use to optimize telescope time. Having five or more targets whose secondary transits could all be observed within the window of our allotted

time at the telescope would be ideal. The project has taken the direction of determining the secondary transit time of potential targets and their availability in the Spring, reviewing the professional literature in the field, and taking a harder look at our data so that we can make convincing proposals for telescope time.

References

[1] John Mason, Exoplanets: Detection, Formation, Properties, Habitability (2008)

[2] P. Cassen, T. Guillot, et al. Extrasolar Planets (2006)

[3] Ch. Broeg, et al., A new algorithm for differential photometry: computing an optimum artificial comparison star (2004)

[4] Luca Rizzi, "WFCAM - The UKIRT Wide Field Camera", http://www.jach.hawaii.edu/UKIRT/

[5] Michael Richmond, "Simple Aperture Photometry by Hand", http://spiff.rit.edu/classes/phys445/lectures